

## **Nanowire-bacteria hybrids for unassisted solar carbon dioxide fixation to value-added chemicals**

Chong Liu<sup>†</sup>, Joseph J. Gallagher<sup>†</sup>, Kelsey K. Sakimoto, Eva M. Nichols, Christopher J. Chang<sup>\*</sup>, Michelle C. Y. Chang<sup>\*</sup>, Peidong Yang<sup>\*</sup>

### **Table of contents:**

#### **Methods**

- 1. Preparation of Si and TiO<sub>2</sub> nanowire arrays**
- 2. Electrochemical and photoelectrochemical (PEC) characterization**
- 3. Integration of electrodes with bacterium *S. ovata***
- 4. Product analysis of acetate production**
- 5. Numerical simulation**
- 6. *E. coli* culturing and biosynthesis of value-added chemicals**
- 7. Quantification of production experiments**

#### **Additional discussion**

- 1. Medium recipes for *S. ovata* culturing**
- 2. Single cell electrochemical activity of CO<sub>2</sub> reduction**
- 3. Derivation of mass transport model in nanowire array**
- 4. Reduced Faradic efficiency in aerobic bacterial catalyzed CO<sub>2</sub> reduction**
- 5. Process design to couple solar-powered CO<sub>2</sub>-reduction with *E. coli*-catalyzed biosynthesis**
- 6. Construction of plasmids**
- 7. Theoretical number of acetate molecules needed to synthesize one product molecules  $N_{\text{acetate,theoretical}}$**

#### **Supplementary figures**

- 1. Electrochemical and photoelectrochemical (PEC) setup**
- 2. Electrochemical CO<sub>2</sub> reduction using the nanowire-bacteria hybrid electrode**
- 3. Stable performance of the nanowire-bacteria hybrid photocathode for solar CO<sub>2</sub> reduction**
- 4. Isotope labeling experiment of CO<sub>2</sub>-fixation with nanowire-bacteria hybrids**
- 5. Enhanced O<sub>2</sub> tolerance from the nanowire-bacteria hybrid electrode**
- 6. Electrochemical measurement of nanowire/Pt electrode with no bacteria loading**
- 7. Synthetic enzymatic pathways for the biosynthesis of target organic compounds**
- 8. Plasmids and primers used in this study**

**9. Production of target organic molecules with genetically engineered *E. coli* strains**

**10. Strategies to alleviate Faradic efficiency decrease for aerobic CO<sub>2</sub> reduction with anaerobes**

**Additional references**

## Methods

### Preparation of Si and TiO<sub>2</sub> nanowire arrays

Silicon (Si) nanowire arrays were fabricated using reactive-ion etching of patterned single-crystalline Si wafers, based on a previous report<sup>22</sup>. To obtain Si nanowire photocathodes with enhanced performance, a thin, highly doped  $n^+$  layer was formed on the surface of the lightly doped  $p$ -Si nanowires for better photovoltage output, similar to the approach reported before.<sup>22,34</sup> In addition, a 30 nm conformal-coated TiO<sub>2</sub> layer was deposited at 300 °C in a home-built atomic layer deposition (ALD) setup in order to maintain stable performance in a pH neutral electrolyte for prolonged periods of time<sup>35</sup>. Moreover, about 10 nm Ni was quasi-conformal sputtered (Edwards, Inc.) onto the electrode, to enhance the charge transfer from the electrode to the bacteria. Similar co-deposition of Pt and Ni was realized for the oxygen-tolerant nanowire-bacteria composite electrode. On the other hand, titanium oxide (TiO<sub>2</sub>) nanowire photoanodes were synthesized *via* hydrothermal methods according to literature<sup>22,36</sup>. After growth, the nanowire electrode was annealed in air for 30 min at 450 °C, and coated with 10 nm TiO<sub>2</sub> *via* ALD to enhance photoresponse<sup>37</sup>. The resultant TiO<sub>2</sub> nanowire photoanode absorbs UV light of the solar spectrum and is capable to oxidize water at neutral pH condition.

### Electrochemical and photoelectrochemical (PEC) characterization

All experiments were performed within a set of custom-built PEC cells, whose basic structure is shown in Supplementary Fig. 1a. The setup is a two-chamber PEC cell, with the working electrode and reference electrode (Ag/AgCl, 1M KCl, CH Instruments, Inc.) in one chamber and the Pt wire counter electrode in the other chamber. A Nafion 117 membrane (Sigma-Aldrich) separates the two chambers. Each chamber has a gas inlet/outlet. The purging gas for each chamber can be independently defined. A peristaltic pump (IDEX Health & Science LLC) is used for media exchange via a solution inlet port in each chamber. Each chamber contains a quartz window for PEC experiments. During experiments the setup was left at ambient temperature, which fluctuated between 20 ~ 26 °C. For unassisted solar-driven CO<sub>2</sub> reduction, shown in Fig. 2e, a third photoanode chamber was connected to the working electrode chamber to accommodate a photoanode of the same surface area as the photocathode. A second Nafion 117 membrane separated the two chambers (Supplementary Fig. 1b).

Electrochemical and PEC measurements were performed using Gamry Interface 1000 potentiostats. The uncertainty of voltage reported here is about 30 mV. The pH of the brackish water solution is typically between 6.3 ~ 6.7 during the measurement. Since the reported voltage is *versus* reversible hydrogen electrode (RHE), the following calculation was used:

$$V \text{ vs. RHE (volt)} = V \text{ vs. Ag/AgCl (volt)} + 0.209 \text{ (volt)} + 0.059 \times \text{pH}$$

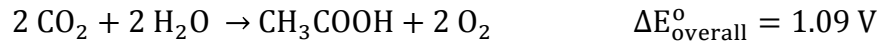
The overpotential  $\eta$  for CO<sub>2</sub> reduction into acetic acid is defined as the voltage difference between the applied electrochemical bias and the standard electrochemical potential for CO<sub>2</sub> reduction into acetic acid:

$$\eta \text{ (volt)} = V \text{ vs. RHE (volt)} + 0.143 \text{ (volt)}$$

Collimated light from a 300W Xenon lamp with AM 1.5G filter (Newport, Corp.) was applied for the measurement of unassisted solar-powered CO<sub>2</sub> fixation, while a 740 nm uniform illumination LED (Mightex Systems, 21 mW/cm<sup>2</sup>) was applied for the measurement of Si nanowire-bacteria photocathode (Supplementary Fig. 3). The energy conversion efficiency of the unassisted solar-powered CO<sub>2</sub> reduction was calculated according to the following equation:

$$\text{energy conversion efficiency (100\%)} = \frac{1.09 \text{ V} \times i(\text{A} \cdot \text{cm}^{-2})}{0.1 \text{ W} \cdot \text{cm}^{-2}}$$

Here  $i(\text{A} \cdot \text{cm}^{-2})$  is the current density of the electrode,  $100 \text{ mW} \cdot \text{cm}^{-2}$  the light intensity of simulated sunlight, and 1.09 V the thermodynamic potential needed to reduce CO<sub>2</sub> into acetate<sup>38</sup>:



### **Integration of electrodes with bacterium *S. ovata***

An inoculum of *S. ovata* was grown under strict anaerobic conditions in a Balch tube at 30 °C. For autotrophic growth of *S. ovata*, hydrogen was used as the electron donor (80% H<sub>2</sub>/20% CO<sub>2</sub>) in brackish water medium modified from the DSMZ-recommended growth medium (DSMZ 311) (see Supplementary Note). Such a “phosphate-enhanced” medium helps the mass transport of protons during electrochemical CO<sub>2</sub> reduction<sup>39</sup>, thus preventing a local pH change near the electrode that may hinder the colonization by *S. ovata*. To achieve higher acetic acid concentrations, a slightly modified M9-MOPS minimal medium was used (see Supplementary Note). *S. ovata* was gradually adapted to growth in M9-MOPS medium. The medium was functional for solar-driven CO<sub>2</sub> reduction, achieving an acetic acid concentration of ~6 g/L (~100 mM).

Incorporation of bacteria into the electrode was realized within the electrochemical cells using organic-free minimal medium, similar to previous report.<sup>28</sup> Unless specifically mentioned, the sparging gas is 20% CO<sub>2</sub>/80% N<sub>2</sub>, and the medium solution contains no organic carbon source except trace vitamin supplement. In general, 10% inoculation was conducted in the cathode chamber of assembled electrochemical cell, where the cathode/photocathode was constantly biased at -0.1 V vs. RHE. The dispersion was cultured for 12 hours under 80% H<sub>2</sub>/20% CO<sub>2</sub> environment, and 2/3 of the electrolyte was replaced with fresh medium. Then the culture was incubated for 24 hours under 20% CO<sub>2</sub>/80% N<sub>2</sub>, and again 2/3 of the electrolyte was replaced with fresh medium. At this stage the electrochemical bias was maintained, and the nanowire cathode acted as the sole electron donor for the bacteria metabolism. After two more cycles of this medium exchange procedure, the nanowire-bacteria hybrids electrode could be obtained in the cathode chamber with minimal planktonic cells suspended in the bulk solution. Such a nano-bio hybrids are ready for detailed characterization.

After the experiment, the Si nanowire-bacteria hybrid electrode was subject to SEM characterization. In particular, critical point drying (Tousimis, Inc.) was applied for the nanowire electrode samples to minimize the effect of the capillary force. The cell loading density was determined by counting the number of cells within a given area of the SEM images. Four replicates were performed for each condition ( $n = 4$ ), and more than 5000 cells were counted in each replicate. In the case of the planar electrode, the electrode area was directly measured from a top-down view in SEM. In the case of the nanowire-bacteria composite electrode, cross-section SEM images were taken, and it was assumed that the visible cells in the SEM images are only within one unit cell of the nanowire array lattice (2  $\mu\text{m}$ ). Based on this assumption, the cell loading density over the projected electrode was determined.

Oxygen tolerance measurements were performed under similar conditions as described above. *S. ovata* was introduced into the working electrode chamber, and the nanowire-bacteria hybrids were formed under a constant electrochemical bias (-0.2 V vs. RHE for Fig. 3b). Then the purging gas was switched to  $\text{O}_2/\text{CO}_2/\text{N}_2$  (21:10:69), and the electrochemical cell was tested for five more days, during which time the composition of the solution was analyzed twice.

### Product analysis of acetate production

Aliquots of the electrolyte were periodically sampled during the experiment. During the sampling process, the potentiostat stopped recording data temporarily, which results in the gaps in the curves shown. The production of acetate was analyzed by quantitative proton nuclear magnetic resonance ( $^1\text{H}$ -qNMR) spectroscopy, with sodium 3-(trimethylsilyl)-2,2',3,3'-tetradeuteropropionate (TMSP-d4, Cambridge Isotope Laboratories, Inc.) as the internal standard. Trace amounts of formic acid (~0.1 mM) were occasionally observed, and there was not a measurable concentration of 2-oxobutyrate as reported in previous literature,<sup>28</sup> which may relate to the modified medium composition applied in current study. For the isotope labeling experiment,  $^{13}\text{C}$ -labeled bicarbonate was used, and the same procedure was applied. Both  $^1\text{H}$ -qNMR and  $^{13}\text{C}$ -NMR techniques were applied to analyze the end product. Because the purging  $\text{CO}_2/\text{N}_2$  mixture is not  $^{13}\text{C}$  labeled, not all of the produced acetate molecules are  $^{13}\text{C}$ -labeled.

The concentration of the major product, acetic acid, was measured before and after the experiment. The Faradic efficiency of acetate production,  $X_{\text{acetate}}$ , is calculated based on the following equation:

$$X_{\text{acetate}} = \frac{\Delta C_{\text{acetic acid}} (\text{mol} \cdot \text{L}^{-1}) \times V_{\text{solution}} (\text{L}) \times 8 \times F (\text{C} \cdot \text{mol}^{-1})}{\int i (\text{A} \cdot \text{cm}^{-2}) \times A (\text{cm}^2) dt}$$

Here  $\Delta C_{\text{acetic acid}} (\text{mol} \cdot \text{L}^{-1})$  is the acetic acid concentration difference between two sampling points,  $V_{\text{solution}} (\text{L})$  is the volume of working electrode chamber,  $F (\text{C} \cdot \text{mol}^{-1})$  is the Faraday constant, and  $\int i (\text{A} \cdot \text{cm}^{-2}) \times A (\text{cm}^2) dt$  is the amount of charge that has been passed through the working electrode. No gas bubbles were visible on the electrode when *S. ovata* was introduced.

## Numerical simulation

Numerical simulation of the O<sub>2</sub> mass transport within the nanowire array was performed using the COMSOL Multiphysics finite-element-analysis software package. In the simulation, only the mass transport of O<sub>2</sub> is accounted for. As shown in the Tafel plots of Fig. 2d, the Tafel slopes of the nanowire and planar electrodes loaded with bacteria are the same, which indicates that proton and bicarbonate mass transport are not rate limiting in the experiment. A constant diffusion layer thickness ( $L_{diff}$ ) was assumed to be 500  $\mu\text{m}$ . Attempts to change  $L_{diff}$  (from 50 to 5000  $\mu\text{m}$ ) did not yield significant differences in simulation results. The O<sub>2</sub> concentration at the nanowire surface ( $C_{surface}$ ) was calculated from the Nernst equation based on the potential applied to the electrode (-0.2 V vs. RHE). The diffusion coefficient of O<sub>2</sub> gas ( $D_{oxygen}$ ) is  $1.99 \times 10^{-5}$  cm<sup>2</sup>/sec (at 298 K), and the saturated concentration of O<sub>2</sub> ( $C_{max}$ ) is 0.259 mmol/L (at 298 K, equilibrated with air). The simulated nanowire has a 1  $\mu\text{m}$  diameter, 30  $\mu\text{m}$  length, and 2  $\mu\text{m}$  periodicity (square lattice, periodic boundary condition). Because of the large difference in length scale between the diffusion layer and the length of nanowire, two separate domains were applied.

## *E. coli* culturing and biosynthesis of value-added chemicals

Electrocompetent *E. coli* BW25113 were transformed with appropriate plasmids, as shown in Fig. 4b and Supplementary Fig. 8. The cells were plated on LB plates containing appropriate antibiotics. After overnight incubation at 37 ° C, colonies were picked into selective LB broth media. After 8 ~ 12 hours of growth, the cells were inoculated 1:100 into selective M9-MOPS media containing 1% (w/v) glucose. The culture was then sequentially grown in M9-MOPS-glucose again, M9-MOPS with 50 mM sodium acetate (twice), and finally transferred to the culture flasks that contain solar-derived M9-MOPS acetate medium (90 ~ 100 mM) for production experiments. The solar-derived acetate medium was generated in the electrochemical cell at aerobic conditions (21% O<sub>2</sub>/10% CO<sub>2</sub>/69% N<sub>2</sub>) under simulated sunlight, and pumped out for biosynthesis. All production experiments were carried out in triplicate.

*n*-Butanol production experiments were performed as reported previously under microaerobic condition<sup>29</sup>. The cells were inoculated to an OD<sub>600nm</sub> of 0.05 in 250 mL baffled screw-top anaerobic culture flasks containing 50 mL media supplemented with 50  $\mu\text{g}/\text{ml}$  carbenicillin and 25  $\mu\text{g}/\text{ml}$  chloramphenicol and kanamycin. The cells were grown aerobically (shaking at 200 rpm with the screw-caps loose) at 37 ° C to an OD<sub>600nm</sub> of 0.3 ~ 0.4, at which point the cultures were induced by adding 1mM IPTG and 0.2% L-arabinose. At induction, the caps were closed tightly to prevent butanol evaporation. The cultures were then maintained at 30 ° C with shaking (200 rpm) for 5 days. Every 24 hours, the flasks were opened to equilibrate with room atmosphere, and 2 mL culture samples were removed for butanol and acetate analysis. The samples were cleared of cells by centrifuging at 14000 rpm for 10 min in a table-top microcentrifuge, transferred to new tubes and frozen at -80 ° C for later analysis. Isoprenoid production experiments

were conducted similarly under aerobic conditions<sup>40</sup>. Here, cells were inoculated to an OD<sub>600nm</sub> of 0.05 in 250 mL baffled culture flasks containing 40 mL media supplemented with 50 µg/ml carbenicillin and 25 µg/ml chloramphenicol. The cultures were induced at an OD<sub>600nm</sub> of 0.2 ~ 0.3 by adding 1mM IPTG. At induction, an organic overlay of 10 mL dodecane was added to each flask. Every 24 hours, a 1 mL sample of the organic overlay and a 1 mL sample of the culture were harvested. A similar protocol at aerobic condition was used for PHB production<sup>31</sup>. Cells were inoculated to an OD<sub>600nm</sub> of 0.05 in 250 mL baffled culture flasks containing 50 mL medium supplemented with 25 µg/ml chloramphenicol and kanamycin. The cultures were induced at an OD<sub>600nm</sub> of 0.3 ~ 0.4 by adding 1mM IPTG and 0.2% L-arabinose. At the end of the 5-day experiment, 40 mL of culture were harvested by centrifuging at 9800 x g for 5 min. 1 mL of cleared culture media was retained for acetate analysis. The cell pellets were re-suspended in 5 mL of deionized water, transferred to pre-weighed 20 mL glass scintillation vials and lyophilized.

### Quantification of production experiments

Detailed analysis methods for the organic compounds have been reported<sup>29,40,41</sup>. *n*-Butanol was measured using a Trace GC Ultra (Thermo Scientific) with an HP-5MS column (0.25 mm × 30 m, 0.25 µm film thickness, J & W Scientific), after extraction with an equal-volume of toluene (500 µL) containing the isobutanol internal standard (100 mg/L). For isoprenoid quantification, 250 µL of the dodecane layer was mixed with 250 µL ethyl acetate containing 5 mg/L trans-caryophyllene as an internal standard. The samples were analyzed using the same instrument described above. Compounds were identified by comparison of the full mass spectrum to authentic standards (butanol) or library compounds (isoprenoids). For quantification, the peak area of the compounds of interest was compared to the peak areas of an authentic standard calibration curve (butanol) or the peak area of the internal standard (isoprenoids). To analyze for PHB content, dry lyophilized cell samples of known weight were treated with conc. H<sub>2</sub>SO<sub>4</sub> at 90 °C for 60 min to convert PHB into its monomer, crotonic acid. Samples were analyzed by liquid chromatography (1200 Series, Agilent Technologies) using an Aminex HPX-87H column (BioRad, Hercules, CA) with 7 mM H<sub>2</sub>SO<sub>4</sub> as the mobile phase and acrylic acid as the internal standard. The eluent was monitored by UV at 214 nm. Acetate was quantified using an Agilent 1200 Series HPLC (Santa Clara, CA) equipped with a Phenomenex Rezex RFQ Fast Fruit H+ column (100 x 7.80mm) (Torrance, CA), by mixing culture media samples (450 µL) with a 4% (v/v) valeric acid internal standard (50 µL). Acetate and valeric acid were detected using a diode array detector by monitoring absorbance at 210 nm. To quantify the production yield X<sub>product</sub> of the target compounds, a theoretical production scenario is assumed (see Supplementary Note), and X<sub>product</sub> was calculated based on the consumption of acetate.

## Additional discussions

### Medium recipes for *S. ovata* culturing

The composition of the modified medium (“phosphate-enhanced medium”) is as follows per 1000 mL:

K <sub>2</sub> HPO <sub>4</sub>	0.348 g
KH <sub>2</sub> PO <sub>4</sub>	0.227 g
Na <sub>2</sub> HPO <sub>4</sub> •7H <sub>2</sub> O	2.145 g
NaH <sub>2</sub> PO <sub>4</sub> •H <sub>2</sub> O	0.938 g
NH <sub>4</sub> Cl	0.500 g
MgSO <sub>4</sub> •7H <sub>2</sub> O	0.500 g
CaCl <sub>2</sub> •2H <sub>2</sub> O	0.250 g
NaCl	0.918 g
FeSO <sub>4</sub> •7H <sub>2</sub> O	0.002 g
NaHSeO <sub>3</sub>	10 <sup>-7</sup> mol/L
NaHCO <sub>3</sub>	4.000 g
Cysteine-HCl	0.300 g
Na <sub>2</sub> S•9H <sub>2</sub> O	0.300 g
SL-10 trace element solution	1 mL
Vitamin solution	10 mL
Yeast extract	2.000 g

Compared to the DSMZ-recommended growth medium<sup>27</sup>, the concentration of phosphate buffer is increased by 5 times from 3.7 mM to 18.5 mM without changing the overall K<sup>+</sup> and Na<sup>+</sup> concentration. Initial growth of *S. ovata* was performed in the full recipe. For electrochemical and photoelectrochemical experiments, Na<sub>2</sub>S, cysteine-HCl, and yeast extract was omitted to ensure an organic-free medium containing only the trace vitamin supplement. To further enhance the buffer strength with higher acetate titer, a modified M9-MOPS medium was used. Compared to standard M9-MOPS medium 10 mL vitamin solution was added.

## Single cell electrochemical activity of CO<sub>2</sub> reduction

As discussed in the main text and shown in Supplementary Fig. 2d, on average at single cell level each second  $(1.1 \pm 0.3) \times 10^6$  acetate molecules could be generated from electrochemical CO<sub>2</sub> reduction. Such a reaction rate should be compared with the acetogenic metabolism rate of *S. ovata*, and it is concluded that the electrochemical reduction rate of CO<sub>2</sub> reduction is similar as the metabolism rate of *S. ovata*. Literature<sup>27</sup> have shown that when *S. ovata* was grown in standard medium solution, within the first 24 hours of growth up to 20 mM acetate could be produced, and the OD<sub>600</sub> is still less than 1.0. Given this, it is possible to calculate a minimal metabolic rate of the Wood-Ljungdahlii pathway in *S. ovata*, assuming OD<sub>600</sub> = 1.0 throughout the 24-hour growth period:

$$r = \frac{20 \times 10^{-3} \text{ mol} \cdot \text{L}^{-1} \times 6.02 \times 10^{23} \text{ mol}^{-1}}{8 \times 10^{11} \text{ cell} \cdot \text{L}^{-1} \times 24 \times 3600 \text{ s}} = \sim 1.7 \times 10^6 \text{ cell}^{-1} \cdot \text{s}^{-1}$$

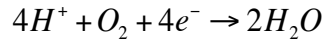
In this calculation, we assume OD<sub>600</sub> 1.0 corresponds to  $\sim 8 \times 10^8$  cells/mL, which is the value for *E. coli*.

Therefore the measured electrocatalytic CO<sub>2</sub> reduction rate is comparable with the value in well-dispersed homogeneous bacteria suspension. This implies that the interfacial charge transfer between the nanowire and bacteria may not be the rate-limiting step, and the measured electrochemical activity may be indicative of the metabolism of the living cells.

## Mathematical model for O<sub>2</sub> concentration profile in the nanowire array

Here, a model to account for O<sub>2</sub> depletion within the proximity of nanowire arrays is provided. In general, the 3-dimensional problem of mass transport is simplified into a one-dimensional model assuming the nanowire array behaves as a porous electrode. The constructed model is based on a previous report for redox mass transport in dye-sensitized solar cells<sup>44</sup>.

The reaction that we are dealing with is oxygen reduction in an aqueous electrolyte:



Assumptions for the model:

1. We treat the nanowire array and the liquid surrounding it as a homogenous porous medium with an averaged redox concentration that is only dependent on the direction along the nanowire. The amount of liquid that is occupied is represented by the dimensionless porosity  $\varepsilon_p$ , which is the volume percentage of the liquid phase.

$$\varepsilon_p = \frac{a^2 - \pi r^2}{a^2}$$

Here  $a$  is the periodicity of the square lattice of the nanowire array, and  $r$  is the radius of the nanowire.

By treating the nanowire array as a homogenous porous medium, only the concentration profile along the nanowire length must be considered. We define this direction as the  $x$ -axis, and the concentration of O<sub>2</sub> is represented as  $C(x)$ .

The boundary of the nanowire array is defined as:

$x > 0$  nanowire array (porous media)

$x < 0$  bulk solution

2. Since an oxygen molecule is charge-neutral and convection of the liquid is minimal within the diffusion layer, the mass transport of oxygen is completely diffusional.
3. The current passing through the nanowire surface could be considered as a homogeneous reaction within the porous media, represented as an "injection rate"  $P_{inj}$ . The relationship between the current density on the surface of the nanowire and  $P_{inj}$  could be written as:

$$P_{inj} = \frac{i \cdot 2\pi r}{Fa^2}$$

Here  $i$  is current density in the unit of [A/m<sup>2</sup>],  $P_{inj}$  is in the unit of [mol/m<sup>3</sup>], and  $F$  is the Faraday constant.

4. The ORR is considered to be first-order dependent on the oxygen concentration at the electrode surface, and the Tafel assumption is applied owing to the large overpotential  $\eta$  applied on the cathode.

Governing equation:

The differential equation for the mass transport of O<sub>2</sub> in the nanowire array could be represented as:

$$D \frac{d^2 C}{dx^2} - \frac{1}{4} \frac{P_{inj}}{\varepsilon_p} = 0$$

As assumed above, the overpotential  $\eta$  versus oxygen reduction is quite large and the current density  $i$  could be represented as the Tafel equation associated with the local O<sub>2</sub> concentration.

$$i = \frac{C(x)}{C_{sat}} \cdot i_{sat} = \frac{C(x)}{C_{sat}} \cdot i_0 e^{\frac{\alpha n F}{RT} \eta}$$

$$C_{sat} = 0.036 \text{ g/L} = 1.125 \times 10^{-3} \text{ mol/L} = 1.125 \text{ mol/m}^3$$

Here  $C_{sat}$  is the saturated oxygen concentration equilibrated with 1 atm O<sub>2</sub> gas. In practice, the partial pressure of O<sub>2</sub> is maintained at 21% in the headspace.  $i_{sat}$  is the current density observed when the mass transport of O<sub>2</sub> is not a limiting factor.

Combining all equations together, the differential equation in the porous media is:

$$D \frac{d^2 C(x)}{dx^2} - \frac{1}{4 \varepsilon_p} \frac{2 \pi r}{F a^2} i_{sat} \frac{C(x)}{C_{sat}} = 0$$

If we define:

$$k^2 = \frac{1}{4 D \varepsilon_p} \frac{2 \pi r}{F a^2} i_{sat} \frac{1}{C_{sat}}$$

Then the equation could be written quite simply:

$$\frac{d^2 C(x)}{dx^2} - k^2 C(x) = 0$$

Considering the fact that  $C(x)$  is decreasing at  $x > 0$ , the solution should be:

$$C(x) \propto e^{-kx}$$

*i.e.* the concentration within the porous media decays exponentially.

Based on the above discussion, it is found that the oxygen concentration profiles in the proximity of planar and nanowire electrodes are different. In the case of a planar electrode, the concentration of oxygen drops almost linearly, consistent with the diffusion layer model (Supplementary Fig. 5a). In contrast, the concentration of oxygen decreases logarithmically in the nanowire array, analogous to a porous electrode (Supplementary Fig. 5b). The fundamental differences in the oxygen concentration profiles of planar and nanowire electrodes allow us to design an integrated bacteria/nanowire electrode for aerobic CO<sub>2</sub> reduction with strictly anaerobic bacteria, as demonstrated in Fig. 3 and Supplementary Fig. 5c.

## Reduced Faradic efficiency in aerobic bacterial catalyzed CO<sub>2</sub> reduction

As mentioned in the main text, when aerobic condition was applied for the nanowire-bacteria hybrids to conduct CO<sub>2</sub> reduction, the Faradic efficiency of acetate production is reduced mostly due to the oxygen reduction reaction. For practical application such a decrease of Faradic efficiency is undesirable. In the following we provide a discussion demonstrating that such a decrease can be alleviated by careful design of nanowire electrodes.

First of all, if people aim to employ anaerobic or oxygen-sensitive strains for CO<sub>2</sub> mitigation, thermodynamics dictate that there must be some energy to be consumed to separate the O<sub>2</sub> from the common aerobic CO<sub>2</sub> feedstock. Based on our discussion, the nanowire-bacteria hybrids are capable of minimizing such energy consumption and approaching to theoretical limit.

As discussed in the theoretical model above, the nanowire array electrode would actively consume the dissolved oxygen in the electrode, resulting in a segment of inactive region where oxygen concentration is too high for the survival of anaerobes (Fig. 3a). So in a first-order approximation, we can consider the percentage loss of acetate yield as:

$$loss = \frac{L_{inactive}}{L_{inactive} + L_{active}} \times 100\%$$

Here  $L_{inactive}$  is the length of nanowire not suitable for anaerobes, and  $L_{active}$  is the region anaerobic enough for the survival of acetogens (“Normal” NW electrode in Supplementary Fig. 10). The measured ~15% loss of acetate yield means that roughly 18% of the nanowire segment is inactive, consistent with our numerical simulation, if a 10<sup>-11</sup> mol/L threshold oxygen concentration is assumed (Fig. 3a).

As implied in our theoretical model and numerical simulation, the absolute length of this inactive segment does not change when varying the total length of the nanowire. Therefore, for a long enough nanowire structure with high aspect ratio ( $L_{active} \rightarrow \infty$ ), the loss of Faradic efficiency can be significantly minimized ( $loss \rightarrow 0$ ), and nano-bio hybrids discussed in this manuscript are relevant for practical application (“Extended” NW electrode in Supplementary Fig. 10).

With increasing aspect ratio of the nanowire array, the mass transport of other species (H<sup>+</sup>, dissolved CO<sub>2</sub>, etc.) in the solution may be hampered if diffusion is the only mechanism. But we can allow the liquid to flow through this nanoelectrode, by taking out the base of the nanowire array to achieve a 3-dimensional network (the nanowire will be interconnected to maintain mechanical strength). In this way the liquid flow provides convective flux for improved mass transport (“Flow-through” NW electrode in Supplementary Fig. 10). Therefore, by careful structural design of the nanowire-bacteria hybrids, it is possible to achieve aerobic CO<sub>2</sub> reduction with anaerobes with minimized Faradic efficiency loss.

## **Process design to couple solar-powered CO<sub>2</sub>-reduction with *E. coli*-catalyzed biosynthesis**

Given that both of solar-powered CO<sub>2</sub>-reduction and *E. coli*-catalyzed biosynthesis can be performed under aerobic environment, it is tempting to have the genetically engineered *E. coli* in the same reactor as the solar-powered CO<sub>2</sub>-reduction via the acetogen, *S. ovata*. However, for two major reasons this is indeed not practical for many commodity chemicals.

First, the low solubility of CO<sub>2</sub> in water indicates that for practical application CO<sub>2</sub> feedstock should be constantly bubbled through the whole CO<sub>2</sub>-reducing reactor. However many commodity chemicals of interest, such as *n*-butanol and isoprenoids discussed in this report, have nontrivial vapor pressure at ambient conditions. So if the biocatalysis is taking place in the same reactor as CO<sub>2</sub>-reduction, the sparging CO<sub>2</sub> gas stream will reduce the yield in the liquid phase, and lead to additional separation cost in the sparging gas phase. Such a scenario is undesirable.

Second, the CO<sub>2</sub>-reducing bacterial catalyst may catabolize the synthesized commodity chemicals. For example,<sup>45</sup> in the case of *n*-butanol it has been reported that during butanol production from a heterologous pathway in *C. ljungdahlii* the desired product is almost completely lost to host metabolism and conversion to butyrate. Therefore it is important to minimize the “cross-talk” between the two processes discussed in current report.

Because of the concerns above, in this report the CO<sub>2</sub>-reduction process and the *E. coli* biocatalysis were performed in separate containers. A mixed-flow or semibatch reactor scheme has been demonstrated, by periodically pumping solar-derived acetate-containing solution from nanowire-bacteria hybrids into the flasks with genetically engineered *E. coli* strains. Such a scheme also represents a modular platform with great flexibility, which simplifies the overall system design.

## Construction of plasmids

Standard molecular biology techniques were used for plasmid construction. *E. coli* DH10B-T1<sup>R</sup> served as the cloning host. All PCR amplifications were carried out with Phusion polymerase (New England Biolabs, Ipswich, MA). Plasmids were assembled using the Gibson method<sup>46</sup>, and sequences were verified using Sanger sequencing (Quintara Biosciences, Berkeley, CA). Detailed descriptions of the plasmids and primers are contained in Supplementary Figure 8.

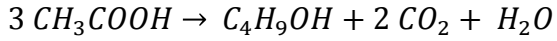
*pBBR1-MCS2-pTrc-ACS\**. The Trc promoter was amplified from pTrc99a<sup>47</sup> using primers pTrcF3 and pTrcR3. The L641P ACS mutant was amplified using primers ACS.Ec.F4 and ACS.Ec.R7. The two PCR products were joined using splicing by overlap extension (SOE) PCR with primers pTrcF3 and ACS.Ec.F7. The resulting PCR fragment was inserted into the EcoRI/SacII sites of pBBR1-MCS2<sup>29</sup>.

*pBT33-phaA.phaB.phaC*. The phaA.phaB operon was amplified from pBT33-Bu2<sup>29</sup> using primers PhaB R6 and PhaA F2. The PCR product was inserted into the NdeI/XhoI sites of pBT33-MSC2-crt<sup>29</sup> to generate pBT33-phaA.phaB-crt. A synthetic version of the phaC gene was amplified using primers PhaC F5 and PhaC R2 and inserted into the SpeI/XhoI sites of pBT33-phaA.phaB-crt to generate pBT33-phaA.phaB.phaC-crt. The Trc-crt region of pBT33-phaA.phaB.phaC-crt was removed by digestion with XhoI and XbaI. The plasmid was closed by inserting the overlapping oligonucleotides PhaABC\_F and PhaABC\_R.

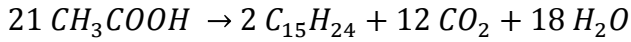
**Theoretical number of acetate molecules needed to synthesize one molecule of product,  $N_{\text{acetate,theoretical}}$**

To derive  $N_{\text{acetate,theoretical}}$  the following ideal scenarios are considered for specific products.

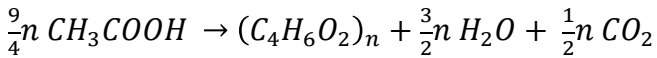
*n*-butanol:



isoprenoids:

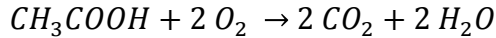


PHB:

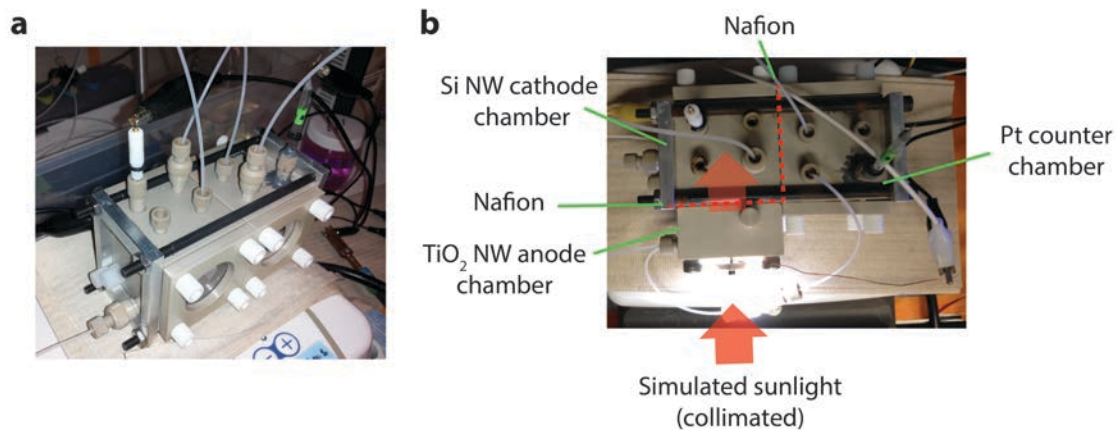


The above equations are considered as the biocatalytic reactions of maximum efficiency, based on the following reasoning:

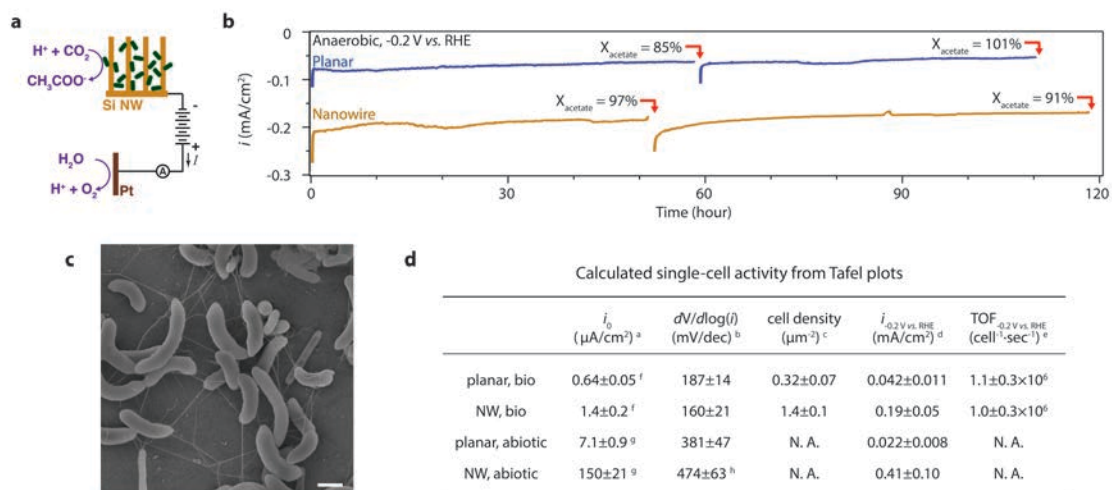
1. The reactant of biocatalysis should be acetic acid, and the end products should be the target molecule,  $\text{CO}_2$ , and  $\text{H}_2\text{O}$ .  $\text{CO}_2$  and  $\text{H}_2\text{O}$  are considered because they cannot be further metabolized by *E. coli*.
2. In the above equation no  $\text{O}_2$  molecules are considered. Any metabolism involving  $\text{O}_2$  molecules can be considered as a linear combination between the above equation and the “combustion” reaction between acetic acid and  $\text{O}_2$ :



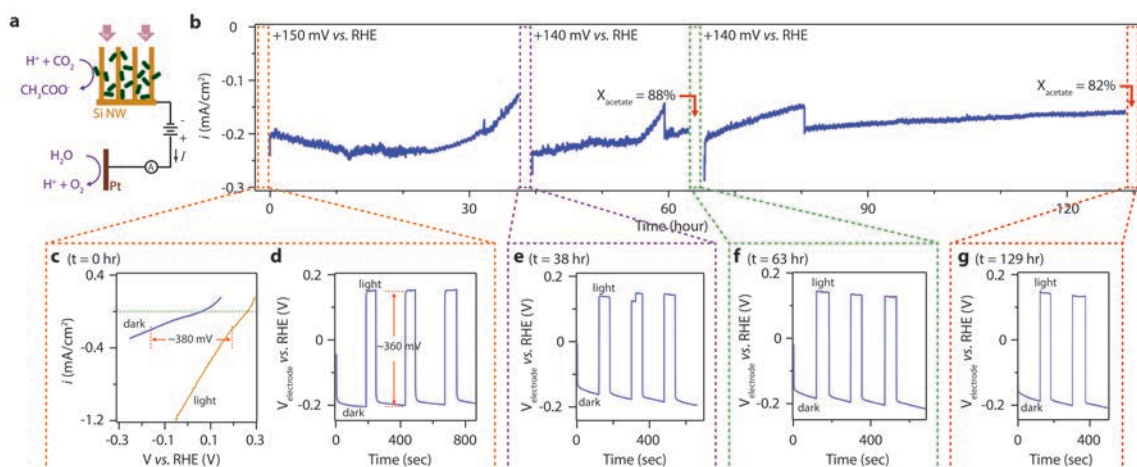
Therefore the theoretical maximum conversion efficiency is based on an  $\text{O}_2$ -free reaction that involves only acetic acid, target molecules,  $\text{CO}_2$ , and  $\text{H}_2\text{O}$ . Based on these equations,  $N_{\text{acetate,theoretical}}$  is 3, 10.5, and 2.25 for *n*-butanol, isoprenoid compounds, and PHB biopolymer (Supplementary Fig. 9b).



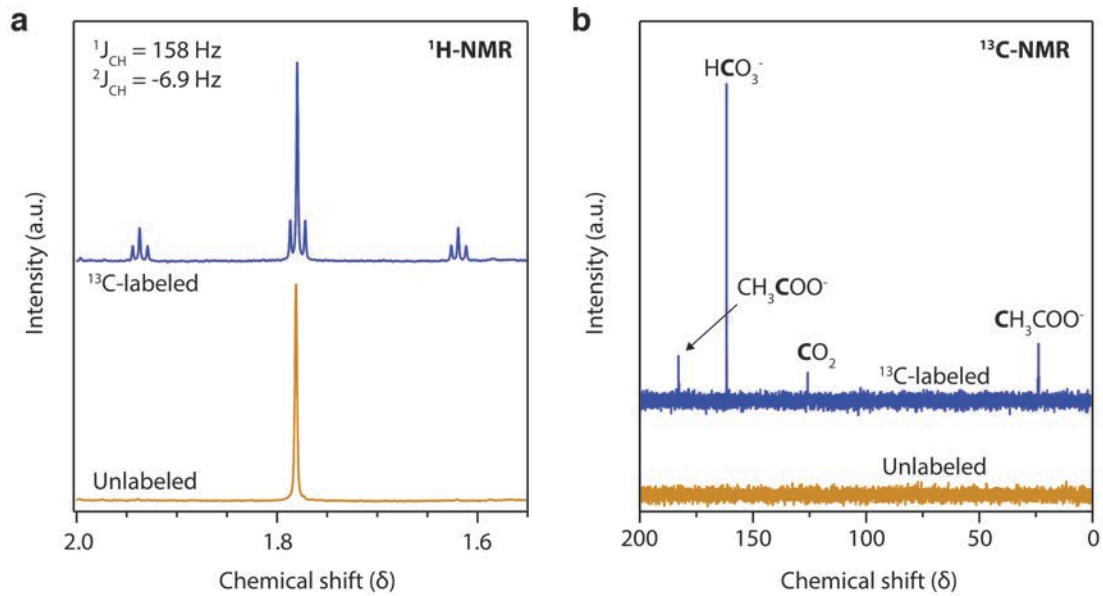
**Supplementary Figure 1 | Electrochemical and photoelectrochemical (PEC) setup. a,** Image of the two-chamber electrochemical setup for CO<sub>2</sub> reduction with nanowire-bacteria hybrid photocathode. **b,** Three-chamber PEC setup for unassisted solar CO<sub>2</sub> reduction using the integrated system. Here, one collimated light beam illuminates first a TiO<sub>2</sub> nanowire photoanode (through its back side), second the Nafion membrane that separates the photocathode and photoanode chambers, and finally the Si nanowire-bacteria photocathode. The Pt counter electrode chamber was used during the incubation period of integrating *S. ovata* into the Si electrode.



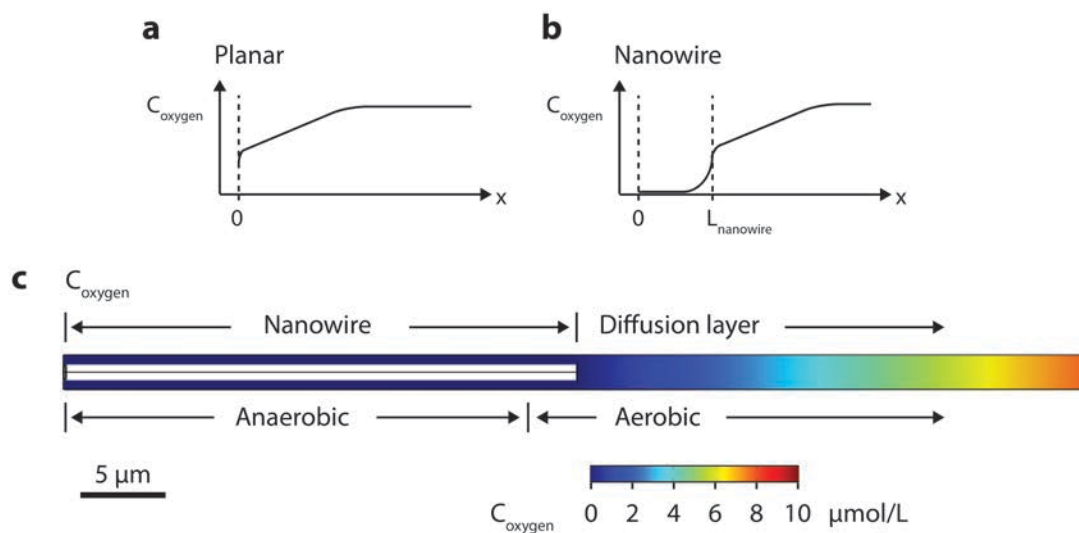
**Supplementary Figure 2 | Electrochemical CO<sub>2</sub> reduction using the nanowire-bacteria hybrid electrode.** **a**, Schematic of bacteria-catalyzed CO<sub>2</sub> reduction with a Si nanowire cathode. **b**, Si nanowire-bacteria hybrid electrode possesses high reaction rate of electrochemical CO<sub>2</sub> fixation and acetate production compared to its planar counterpart. Degenerately doped Si was applied to minimize the serious resistance. The product selectivity to acetate ( $X_{\text{acetate}}$ ) during each time interval is displayed. **c**, Representative SEM images of *S. ovata*. Geometrical information for *S. ovata* was derived to calculate the single-cell activity. **d**, Electrochemical data summarized from Fig. 2d ( $n = 2$ ). The selectivity of acetate production  $X_{\text{acetate}}$  is larger than 70% for all reported biotic data. As shown in the table, the Tafel slope  $dV/d\log(i)$  is distinctly different in the presence of bacteria, indicating a difference of reaction mechanism between abiotic proton reduction and bio-catalyzed CO<sub>2</sub> reduction. <sup>a</sup> Exchange current density  $i_0$  per geometric electrode area. <sup>b</sup> Tafel slope, which is a measure of the apparent kinetic barrier. <sup>c</sup> *S. ovata* cell loading density per geometric electrode area. <sup>d</sup> Current density measured at -0.2 V vs. RHE. <sup>e</sup> Single-cell turnover frequency (TOF) measured at -0.2 V vs. RHE. <sup>f</sup> Measured based on the electrochemical potential of acetic acid formation (+0.143 V vs. RHE). <sup>g</sup> Measured based on the electrochemical potential of proton reduction (0 V vs. RHE). <sup>h</sup> The Tafel slope may be convoluted with the mass transport when the current density is high. The scale bar in **c** is 1  $\mu\text{m}$ .



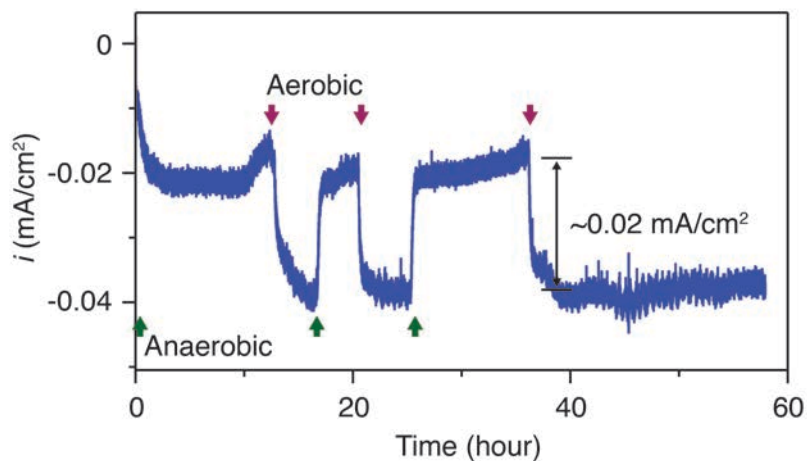
**Supplementary Figure 3 | Stable performance of the nanowire-bacteria hybrid photocathode for solar CO<sub>2</sub> reduction.** **a**, Setup schematic for solar-driven CO<sub>2</sub> reduction with Si nanowire-bacteria hybrid as the photocathode. **b**, Representative data for long term testing of solar CO<sub>2</sub> reduction under constant bias (0 ~ 38 hours: +150 mV vs. RHE, 38 ~129 hours: +140 mV vs. RHE),  $n = 3$ . **c**, Linear scan voltammetry curves (10 mV/sec) of the integrated photocathode in dark and light. The stability of the hybrid electrode was tested by measurement of photovoltage output at different intervals during the experiment: **d**,  $t = 0$  hour; **e**,  $t = 38$  hours; **f**,  $t = 63$  hours; **g**,  $t = 129$  hours. The photovoltage was measured chronopotentiometrically at 0.2 mA/cm<sup>2</sup> with chopped illumination (740 nm LED light source). The photovoltages measured over the period of 5 days were stable and consistent with the value extracted from **c**.



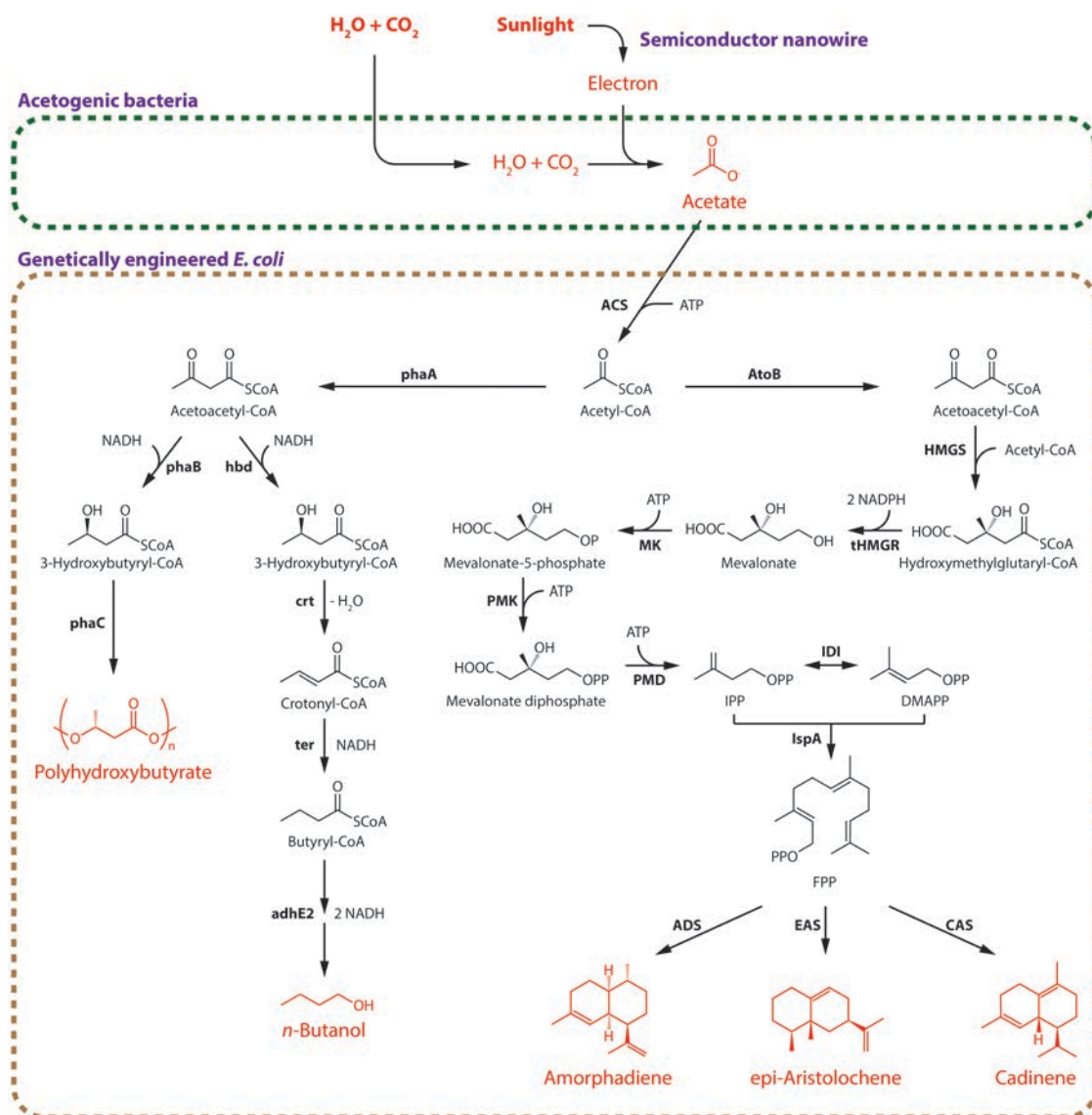
**Supplementary Figure 4 | Isotope labeling experiment of  $\text{CO}_2$ -fixation with nanowire-bacteria hybrids.** **a**,  $^1\text{H-NMR}$  spectra of acetate produced from unlabeled and  $^{13}\text{C}$ -labeled electrolyte. For  $^{13}\text{C}$ -labeled samples, the high abundance of  $^{13}\text{C}$  in the acetate magnifies  $^1J_{\text{CH}}$  and  $^2J_{\text{CH}}$  coupling, resulting in the satellite peaks in the spectrum. **b**,  $^{13}\text{C-NMR}$  spectra of acetate produced from unlabeled and  $^{13}\text{C}$ -labeled electrolyte. With the addition of  $\text{NaH}^{13}\text{CO}_3$ , the  $^{13}\text{C}$ -signal is strongly enhanced in bicarbonate, dissolved  $\text{CO}_2$ , and the produced acetate molecules.



**Supplementary Figure 5 | Enhanced  $\text{O}_2$  tolerance from the nanowire-bacteria hybrid electrode.** Scheme of the  $\text{O}_2$  concentration profile near the planar (**a**) and nanowire array (**b**) electrodes. A detailed derivation is available in the Supplementary Information. **c**, An additional simulation result of the  $\text{O}_2$  concentration profile near a nanowire array electrode. Notably here a wider region of the diffusion layer is plotted in a linear scale of  $C_{\text{oxygen}}$ , highlighting the linear decrease of  $\text{O}_2$  concentration within the diffusion layer.



**Supplementary Figure 6 | Electrochemical measurement of nanowire/Pt electrode with no bacteria loading.** Pt-loaded Si nanowire electrode without *S. ovata* was tested in the same medium solution as Fig. 3 at -0.2 V vs. RHE. Same as Fig. 3, the sparging gas was switched between anaerobic (20% CO<sub>2</sub>/80% N<sub>2</sub>) and aerobic (21% O<sub>2</sub>/10% CO<sub>2</sub>/69% N<sub>2</sub>). The increased current density ( $\sim 0.02$  mA/cm<sup>2</sup>) under aerobic environments is due to the oxygen reduction reaction, which contributes to the decrease of Faradic efficiency to yield acetate measured in Fig. 3b.



**Supplementary Figure 7 | Synthetic enzymatic pathways for the biosynthesis of target organic compounds.** Each product was produced in a different genetically engineered *E. coli* strain. All pathways begin with acetyl-CoA, which was generated by the activation of solar-derived acetate. In addition to these described pathways, some of the acetyl-CoA are expected to be diverted into the TCA cycle for redox balancing. IPP, isopentenyl pyrophosphate; DMAPP, dimethylallyl pyrophosphate. ACS, acetyl-CoA synthase; *phaA*, acetoacetyl-CoA thiolase/synthase; *hbd*, *phaB*, 3-hydroxybutyryl-CoA dehydrogenase; *crt*, crotonase; *ter*, *trans*-enoyl-CoA reductase; *adhE2*, bifunctional butyraldehyde and butanol dehydrogenase; *phaC*, PHA synthase; *AtoB*, acetyl-CoA acetyltransferase; *HMGS*, hydroxymethylglutaryl-CoA synthase; *tHMGR*, truncated hydroxymethylglutaryl-CoA reductase; *MK*, mevalonate kinase; *PMK*, phosphomevalonate kinase; *PMD*, phosphomevalonate decarboxylase; *IDI*, isopentenyl diphosphate-isomerase; *IspA*, farnesyl diphosphate synthase; *ADS*, amorphadiene synthase; *EAS*, epi-aristolochene cyclase; *CAS*, cadinene synthase.

**a**

## Plasmids used in this study

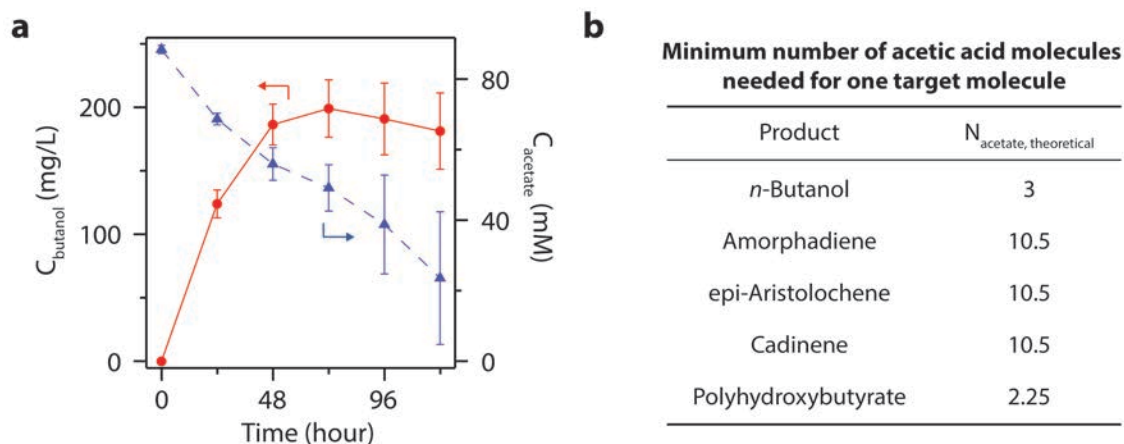
Plasmid	Description	Source
pBT33-Bu2	<i>phaA.hbd (Ara), crt (Trc), araC, Cm<sup>r</sup>, p15a</i>	Ref. 29
pCWori-ter.adhE2	<i>ter.adhE2 (double Tac), laclq, Cb<sup>r</sup>, ColE1</i>	Ref. 29
pBBR1-MCS2-pTrc-ACS*	<i>ACS* (Trc), laclq, Km<sup>r</sup>, pBBR</i>	this study
pAM45	<i>AtoB.HMGS.HMGR (lacUV5), MK.PMK.PMD.IDI.ispA (lacUV5), Cm<sup>r</sup>, p15a</i>	Ref. 40
pADS	<i>ADS (Trc), laclq, Cb<sup>r</sup>, ColE1</i>	Ref. 42
pCAS	<i>CAS (Trc), laclq, Cb<sup>r</sup>, ColE1</i>	Ref. 43
pEAS	<i>EAS (Trc), laclq, Cb<sup>r</sup>, ColE1</i>	Ref. 43
pBT33-phaA.phaB.phaC	<i>phaA.phaB.phaC (Ara), araC, Cm<sup>r</sup>, p15a</i>	this study

**b**

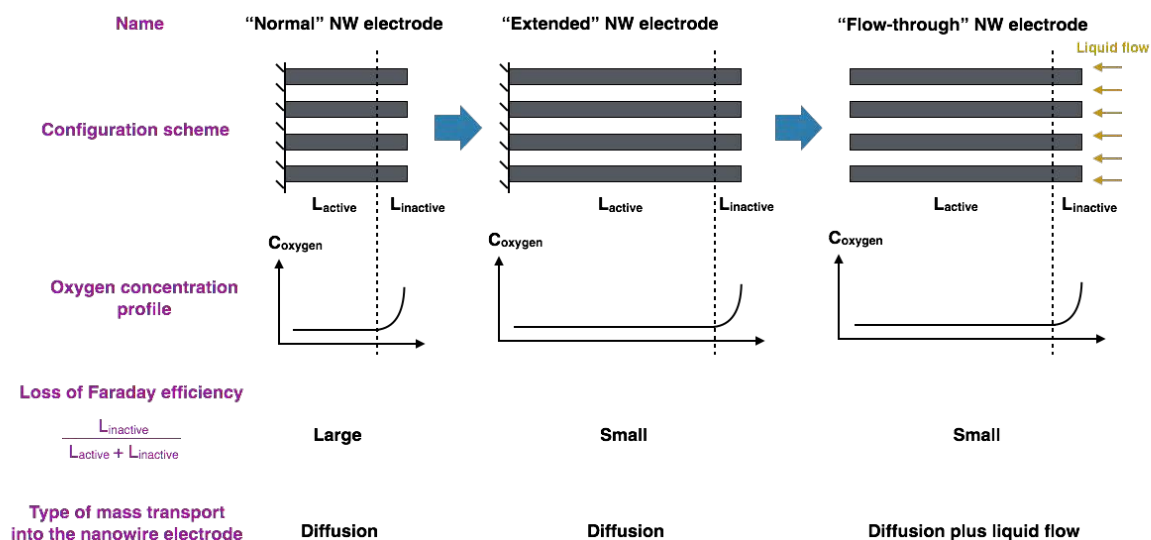
## Primer information for plasmid construction

Primer	Sequence
pTrcF3	CACTAGGAATTCCGACTGCACGGTGCACCAATGCTTCT
pTrcR3	ACTAGTGGATCCTGTGCTGGTGCCTAGGCTGTTTCTGTGTGAAATTGTTATCC
ACS.Ec.F4	AGGCACCAGCACAGGATCCACTAGTTTTAAGAAGCAATATCATATGAGCCAAATT CACAAACACACC
ACS.Ec.R7	GCTCCACCGCGGTGGCGGCCGCTCTAGA TTACGATGGCATCGCGATAGCCTGC
PhaA F2	AAGGAGATATACATATGACTGATGTTGTGATTGTAAGCGCTGCACGTACTGCTGTT GGTAAGTTCGGTGGCTCCCTGGC
PhaB R6	CTCGAGCTCGAGCGGAGGTAGACTAGTTTAGCCCATGTGCAGGCCACCGTTCAG GG
PhaC F5	GGCTAAACTAGTCCGGAGGTATAATTAATGGCGACCGGCAAAGGCGCGG
PhaC R2	ATGCTACTCGAGTCATGCCTTGGCTTTGACGTA
PhaABC_F	CTCGAGACGCTGGTGATCTAGAGTCGACCTGCAGGCATGCAAGCTTGGCTGTTT TGGCGG
PhaABC_R	TCTAGATCACCAGCGTCTCGAGTCATGCCTTGGCTTTGACGTATCGCCAGGCGCG GGTTCG

**Supplementary Figure 8 | Plasmids and primers used in this study.** Detailed information on plasmid construction can be found in the Supplementary Information.



**Supplementary Figure 9 | Production of target organic molecules with genetically engineered *E. coli* strains.** **a**, Time course of *n*-butanol production using solar-derived acetate from the nanowire-bacteria hybrid system. As a representative example, the accumulation of *n*-butanol is accompanied by the consumption of acetate. Due to *n*-butanol evaporation, a slight decrease is observed in butanol concentrations in later days of the experiment. **b**, Display of the theoretical number of acetate molecules needed to synthesize one product molecule  $N_{\text{acetate, theoretical}}$  (see Supplementary Information).



**Supplementary Figure 10 | Strategies to alleviate Faradic efficiency decrease for aerobic CO<sub>2</sub> reduction with anaerobes.** As derived in our theoretical model, the inactive segment of nanowire (NW) array is constant. Therefore with higher aspect ratio of the nanowire, the percentage of inactive segment will be smaller and subsequently the loss of faradic efficiency can be minimized. The option to have a “flow-through” version of the nanowire array facilitates mass transport and further relaxes the design flexibility.

## Additional references

- 34 Boettcher, S. W. *et al.* Photoelectrochemical Hydrogen Evolution Using Si Microwire Arrays. *J. Am. Chem. Soc.* **133**, 1216-1219 (2011).
- 35 Seger, B. *et al.* Using TiO<sub>2</sub> as a Conductive Protective Layer for Photocathodic H<sub>2</sub> Evolution. *J. Am. Chem. Soc.* **135**, 1057-1064 (2013).
- 36 Liu, B. & Aydil, E. S. Growth of Oriented Single-Crystalline Rutile TiO<sub>2</sub> Nanorods on Transparent Conducting Substrates for Dye-Sensitized Solar Cells. *J. Am. Chem. Soc.* **131**, 3985-3990(2009).
- 37 Hwang, Y. J., Hahn, C., Liu, B. & Yang, P. Photoelectrochemical Properties of TiO<sub>2</sub> Nanowire Arrays: A Study of the Dependence on Length and Atomic Layer Deposition Coating. *ACS Nano* **6**, 5060-5069 (2012).
- 38 Drake, H. L. *Acetogenesis*. (Chapman & Hall, 1994).
- 39 Jeremiasse, A. W., Hamelers, H. V. M., Kleijn, J. M. & Buisman, C. J. N. Use of Biocompatible Buffers to Reduce the Concentration Overpotential for Hydrogen Evolution. *Environ. Sci. Technol.* **43**, 6882-6887 (2009).
- 40 Anthony, J. R. *et al.* Optimization of the mevalonate-based isoprenoid biosynthetic pathway in *Escherichia coli* for production of the anti-malarial drug precursor amorpha-4,11-diene. *Metab. Eng.* **11**, 13-19 (2009).
- 41 Karr, D. B., Waters, J. K. & Emerich, D. W. Analysis of Poly- $\beta$ -Hydroxybutyrate in *Rhizobium japonicum* Bacteroids by Ion-Exclusion High-Pressure Liquid Chromatography and UV Detection. *Appl. Environ. Microbiol.* **46**, 1339-1344 (1983).
- 42 Martin, V. J., Pitera, D. J., Withers, S. T., Newman, J. D., Keasling, J. D., Engineering a mevalonate pathway in *Escherichia coli* for production of terpenoids. *Nature Biotechnol.* **21**, 796-802 (2003)
- 43 Martin, V. J., Yoshikuni, Y., Keasling, J. D., The *in vivo* synthesis of plant sesquiterpenes by *Escherichia coli*. *Biotechnol. Bioeng.* **75**, 497-503 (2001).
- 44 Papageorgiou, N., Grätzel, M. & Infelta, P. P. On the relevance of mass transport in thin layer nanocrystalline photoelectrochemical solar cells. *Solar Energy Mater. & Solar Cells* **44**, 405-438 (1996).
- 45 Kopke, M. *et al.* *Clostridium ljungdahlii* represents a microbial production platform based on syngas. *Proc. Natl. Acad. Sci. U.S.A.* **107**, 13087-13092 (2010).
- 46 Gibson, D. G. *et al.* Enzymatic assembly of DNA molecules up to several hundred kilobases. *Nature Meth.* **6**, 343-345 (2009).
- 47 Amann, E., Ochs, B. & Abel, K.-J. Tightly regulated tac promoter vectors useful for the expression of unfused and fused proteins in *Escherichia coli*. *Gene* **69**, 301-315 (1988).